European Journal of Radiology Open 13 (2024) 100599

Contents lists available at ScienceDirect

European Journal of Radiology Open

journal homepage: www.elsevier.com/locate/ejro

The impact of deep learning image reconstruction of spectral CTU virtual non contrast images for patients with renal stones

Hong Zhu [a], Deyan Kong [a], Jiale Qian [a], Xiaomeng Shi [b], Jing Fan [a,*]

[a] Department of Radiology, Ruijin Hospital, Shanghai Jiao Tong University School of Medicine, 200025, China
[b] CT Imaging Research Center, GE Healthcare China, Shanghai 201203, China

ARTICLE INFO

Keywords:
DECT
CT Urography
Deep learning image reconstruction
Virtual non-contrast image
Renal calculus

ABSTRACT

Purpose: To compare image quality and detection accuracy of renal stones between deep learning image reconstruction (DLIR) and Adaptive Statistical Iterative Reconstruction-Veo (ASIR-V) reconstructed virtual non-contrast (VNC) images and true non-contrast (TNC) images in spectral CT Urography (CTU).
Methods: A retrospective analysis was conducted on images of 70 patients who underwent abdominal-pelvic CTU in TNC phase using non-contrast scan and contrast-enhanced corticomedullary phase (CP) and excretory phase (EP) using spectral scan. The TNC scan was reconstructed using ASIR-V70 % (TNC-AR70), contrast-enhanced scans were reconstructed using AR70, DLIR medium-level (DM), and high-level (DH) to obtain CP-VNC-AR70/DM/DH and EP-VNC-AR70/DM/DH image groups, respectively. CT value, image quality and kidney stones quantification accuracy were measured and compared among groups. The subjective evaluation was independently assessed by two senior radiologists using the 5-point Likert scale for image quality and lesion visibility.
Results: DH images were superior to AR70 and DM images in objective image quality evaluation. There was no statistical difference in the liver and spleen (both $P > 0.05$), or within 6HU in renal and fat in CT value between VNC and TNC images. EP-VNC-DH had the lowest image noise, highest SNR, and CNR, and VNC-AR70 images had better noise and SNR performance than TNC-AR70 images (all $p < 0.05$). EP-VNC-DH had the highest subjective image quality, and CP-VNC-DH performed the best in lesion visibility. In stone CT value and volume measurements, there was no statistical difference between VNC and TNC ($P > 0.05$).
Conclusion: The DLIR-reconstructed VNC images in CTU provide better image quality than the ASIR-V reconstructed TNC images and similar quantification accuracy for kidney stones for potential dose savings.
The study highlights that deep learning image reconstruction (DLIR)-reconstructed virtual non-contrast (VNC) images in spectral CT Urography (CTU) offer improved image quality compared to traditional true non-contrast (TNC) images, while maintaining similar accuracy in kidney stone detection, suggesting potential dose savings in clinical practice.

1. Introduction

With the development of society, environmental pollution, genetic inheritance and changes in various dietary habits have caused more and more diverse factors to form urological diseases in today's society, and most of the clinical manifestations are similar to other systemic diseases. Diseases of the urinary system includes various conditions such as urinary system tumors, urinary stones, hydronephrosis, and cysts. These diseases have a relatively high clinical incidence and are not easily detected or distinguished during initial diagnosis. Some conditions require multiple examinations before a definitive diagnosis can be made.

Urinary stones are one of the most common causes of abdominal pain and hematuria, and CTU is a common examination method to diagnose urinary stones [1,2]. Typical CTU protocols usually include non-contrast scanning, contrast-enhanced corticomedullary phase and excretory phase scanning which involve multiple scans, high radiation doses, and possibly multiple contrast agent injections, and high demands on kidney function, reducing radiation exposure while ensuring clinical diagnosis is of significant clinical value for CTU examinations of the urinary system [3,4]. Also because the lower abdomen contains many

* Corresponding author.
E-mail addresses: zh40423@rjh.com.cn (H. Zhu), kdy04163@rjh.com.cn (D. Kong), qjl04113@rjh.com.cn (J. Qian), colin-shi@hotmail.com (X. Shi), fanfan06009@126.com (J. Fan).

https://doi.org/10.1016/j.ejro.2024.100599
Received 16 April 2024; Received in revised form 13 August 2024; Accepted 27 August 2024

radiation-sensitive organs, it is of great practical and clinical value to reduce the radiation dose of CTU scans while ensuring the accuracy of clinical diagnosis.

By taking advantage of the photon absorption variations of two different energies of materials with high atomic numbers (e.g. iodine), dual-energy CT (DECT) allows selective identification and removal of iodine from reconstructed voxels and the creation of synthesized virtual non-enhanced CT datasets, known as spectral virtual non-contrast (VNC) images which present similar to true non contrast (TNC) scans [5–7]. In CTU scans, VNC images have demonstrated consistent imaging and lesion diagnostic efficacy as the non-contrast scans [6,8].

In recent years, artificial intelligence (AI) has rapidly developed and been applied in the field of medical imaging, including deep learning image reconstruction algorithms applied to the conventional CT scans, as well as the dual-energy spectral imaging (e.g. TrueFidelity™, GE HealthCare). The TrueFidelity™ spectral image reconstruction algorithm uses high-dose high-quality filtered backprojection (FBP) spectral images as learning targets to train the reconstruction of low-dose low-quality image raw data using Convolutional neural network (CNN). The purpose of deep learning reconstruction is to overcome the disadvantage of altering image texture brought by iterative reconstruction algorithms. Phantom studies have shown that compared to iterative reconstruction algorithms, the TrueFidelity™ spectral image reconstruction algorithm can further enhance image quality without changing image texture [9,10].

Deep Learning Image Reconstruction (DLIR) technology, as a novel CT image reconstruction method, can effectively reduce image noise and improve image quality [11–14]. However, there is currently lack of research on the diagnostic performance of VNC images from DECT scans reconstructed using DLIR. Therefore, the purpose of this study is to compare the image quality and accuracy of kidney stone measurements between VNC images from DECT scans with thin-layer DLIR reconstruction and conventional CTU images reconstructed with Adaptive Statistical Iterative Reconstruction-Veo (ASIR-V) including TNC and VNC.

2. Materials and methods

2.1. General information

A total of 70 patients diagnosed with urinary system diseases and underwent routine CTU examination in our hospital between September 2022 and October 2023 were included in the study, excluding patients who had undergone bladder resection or had urinary diversion pouches.

2.2. Protocol and post-processing

All examinations were performed on a 256-slice CT scanner (Revolution Apex CT, GE HealthCare, USA). Patients were instructed to drink sufficient water before the examination to ensure the bladder is expanded. After ensuring bladder filling, an abdominal-pelvic non-contrast scan was performed with patients in a supine position. The parameters were: tube voltage 120 kV, automatic tube current modulation (Smart mA), Noise Index (NI) 8.0 HU. After the non-contrast scan, a contrast-enhanced abdominal-pelvic dual-energy spectral CT scan in the corticomedullary phase (CP) was performed 45 s after contrast injection, with the same scanning range as the non-spectral scan. The tube voltage for the enhanced scan was 80/140 kV, using spectral Assist automatic tube current modulation, Noise Index (NI) 8.0 HU, and controlling the volumetric CT dose index (CTDIvol) within a range of (± 1 mGy) of the conventional non-contrast scan. Subsequently, after emptying the bladder, the patients were asked to drink water, the excretory phase (EP) spectral abdominal-pelvic scan was performed when the bladder was filled again (30–60 min after contrast agent injection). The parameters for this scan were consistent with the corticomedullary phase spectral scan. For contrast enhancement, 80 ml of iodixanol contrast agent (350 mg I/ml, Iohexol, Hengrui Medicine, China) followed by 20 ml of 0.9 % saline solution was injected intravenously into the right cubital at a rate of 1.5–2 ml/s. The scan volumetric CT dose index (CTDIvol) values were recorded for the plain, corticomedullary, and excretory phase scans. The three-phase data was reconstructed with a slice thickness and interval of 1.25 mm. The abdominal-pelvic non-contrast scan was reconstructed using ASIR-V technology with 70 % weight (TNC-AR70 group). The corticomedullary and excretory phase scans were reconstructed using ASIR-V and two levels of DLIR algorithm (DM with the medium level and DH with the high level) to obtain six groups of images (CP-VNC-AR70 group, CP-VNC-DM group, CP-VNC-DH group, EP-VNC-AR70 group, EP-VNC-DM group, EP-VNC-DH group). Data measurements and comparisons were conducted on all seven groups of images, including the true non-contrast scans, using an advanced image workstation (Advantage Workstation 4.7, GE HealthCare, USA).

2.3. Image quality evaluation and stone measurement

Objective Evaluation: The portal vein level was selected to measure the CT values and standard deviations (SD) of the regions of interest (ROI) of the liver and spleen. The bilateral renal portal levels were selected for the right kidney parenchyma and abdominal wall fat. The ROI measurements were replicated to ensure consistent size and position, with the liver ROI size approximately 550 mm^2, spleen ROI size approximately 200 mm^2, subcutaneous fat and kidney ROI size approximately 20 mm^2. Signal-to-Noise Ratio (SNR) and Contrast-to-Noise Ratio (CNR) were calculated during ROI measurements.

$$SNR_{ROI} = \frac{CT_{ROI}}{SD_{ROI}}$$

$$CNR_{ROI} = \frac{CT_{ROI} - CT_{Fat}}{SD_{ROI}}$$

Subjective Evaluation: Two experienced senior radiologists evaluated the abdominal-pelvic images using a double-blind method. They independently scored the images on two dimensions: image quality and lesion visibility, using the 5-point Likert Scale scoring method. For image quality scoring, the scale included 5 points for excellent image quality and diagnostic confidence; 4 points for good image quality and high diagnostic confidence; 3 points for acceptable image quality and diagnostic capability; 2 points for poor image quality and low diagnostic confidence; and 1 point for poor image quality and inability to make a diagnosis. For lesion visibility, the scale included 5 points for excellent display of kidney stones for precise diagnosis; 4 points for clear display of kidney stones for accurate diagnosis; 3 points for good display of kidney stones for diagnosis; 2 points for suboptimal display of kidney stones with blurry lesions; and 1 point for extremely poor display of kidney stones with invisible lesions. A score exceeding 3 points was considered to meet the requirements for radiological diagnosis.

Stone Measurement: The results from CT combined with ultrasound were used as the gold standard to confirm 70 cases of kidney stone patients. For these patients, one physician measured CT values and volumes of kidney stones based on the seven groups of images using the compare software on an advanced image workstation, selecting the maximum level of the stone for CT value measurement on each image. Another physician, used the Auto select tool in the compare software to automatically measure the stone volume in the kidney stone area after two months. The average of the two measurements was taken as the measurement value for stone CT values and volumes.

2.4. Radiation dose calculation

The volumetric CT dose index (CTDIvol) and dose-length product (DLP) from the CT scans were recorded, and the effective dose (ED) was calculated as ED = DLP × K value with K value = 0.015 mSv/(mGy·cm).

Table 1
Scanning parameters.

Parameters	TNC (n = 70)	CP (n = 70)	EP (n = 70)
Tube voltage (kV)	120	80/140	80/140
Tube current mode	Smart mA	GSI Assist	GSI Assist
Collimation (mm)	80	80	80
Scanning mode	Hellical	Hellical	Hellical
Matrix	512 × 512	512 × 512	512 × 512
Thickness (mm)	1.25	1.25	1.25
Reconstruction	AR70	AR70/DM/DH	AR70/DM/DH
$CTDI_{vol}$ (mGy)	9.05 ± 2.63	8.99 ± 2.75	8.99 ± 2.75

TNC: true non-contrast, CP: corticomedullary phase, EP: excretory phase.

2.5. Statistical analysis

All numerical and quantitative data were presented as mean ± standard deviation. Kolmogorov-Smirnov tests confirmed normal distribution for all numerical data. ANOVA was used for inter-group comparisons of the seven objective parameters and stone parameters measurement. If statistical differences were found, post-hoc multiple comparisons were conducted using Levene's test for homogeneity of variances, followed by Dunn-Bonferroni or T3-Dunnett correction. Kruskal-Wallis non-parametric test was used for subjective ratings, with significance set at $P < 0.05$. Bland-Altman analysis was used to assess the deviation in stone CT values and measurements between virtual and true non-contrast scans. Observer agreement and stone measurement consistency were evaluated using Kappa tests, with values between 0.8 and 1.0 indicating excellent agreement, 0.6–0.8 indicating good agreement, 0.4–0.6 indicating fair agreement, and below 0.4 indicating poor agreement. Data analysis was performed using SPSS 26.0 (IBM, USA) statistical software.

3. Results

This study included a total of 70 patients, with 43 males and 27 females, aged 21–82 years with an average age of 56.24 ± 14.51 years. The Body Mass Index (BMI) ranged from 20.94 to 31.56 kg/m^2, with an average BMI of 24.61 ± 2.27 kg/m^2. There were 70 cases of kidney stone patients. The average CTDIvol for routine non-contrast scans was 9.28 ± 2.83 mGy, and for corticomedullary phase and excretory phase spectral scans, the average CTDIvol was 9.25 ± 2.94 mGy.

Table 2
Comparison of objective parameters of virtual non-contrast and real non-contrast images of different phases.

	TNC-AR70	CP-VNC-AR70	CP-VNC-DM	CP-VNC-DH	EP-VNC-AR70	EP-VNC-DM	EP-VNC-DH	F	P
CT (HU)									
Liver	56.23 ± 7.80	57.14 ± 6.20	57.03 ± 6.19	57.09 ± 6.13	58.11 ± 6.98	58.15 ± 6.97	58.27 ± 6.86	0.89	0.50
Spleen	50.65 ± 2.89	50.17 ± 2.70	50.13 ± 2.70	50.16 ± 2.70	50.67 ± 2.48	50.67 ± 2.5	50.79 ± 2.45	0.88	0.51
Kidney	34.71 ± 4.80[e,f,g]	35.83 ± 6.97	35.99 ± 6.91	36.09 ± 6.66	37.5 ± 3.91[a]	38.23 ± 4.64[a]	37.82 ± 3.61[a]	3.72	< 0.001
Fat	− 105.74 ± 8.72[e,f,g]	− 101.58 ± 10.36	− 101.81 ± 9.93	− 102.01 ± 9.64	− 100.17 ± 11.65[a]	− 100.31 ± 11.14[a]	− 100.37 ± 11.00[a]	2.44	0.03
SD (HU)									
Liver	11.65 ± 1.58[b,c,d,e,f,g]	7.92 ± 0.72[a,c,d,f,g]	8.88 ± 0.72[a,b,d,e,g]	6.93 ± 0.61[a,b,c,e,f,g]	7.76 ± 1.04[a,c,d,f,g]	8.63 ± 0.95[a,b,d,e,g]	6.4 ± 0.69[a,b,c,d,e,f]	225.42	< 0.001
Spleen	10.54 ± 1.67[b,c,d,e,f,g]	7.65 ± 0.82[a,c,d,f,g]	8.69 ± 0.84[a,b,d,e,g]	6.81 ± 0.74[a,b,c,e,f,g]	7.33 ± 0.87[a,c,d,f,g]	8.25 ± 0.87[a,b,d,e,g]	6.16 ± 0.75[a,b,c,d,e,f]	147.36	< 0.001
Kidney	9.86 ± 2.12[b,d,e,f,g]	8.43 ± 2.14[a,c,e,g]	9.72 ± 2.16[b,d,e,f,g]	8.39 ± 2.03[a,c,e,g]	7.23 ± 1.58[a,b,c,d,f]	8.44 ± 1.50[a,c,e,g]	6.69 ± 1.31[a,b,c,d,f]	27.38	< 0.001
Fat	8.54 ± 3.02[g]	9.47 ± 4.65[g]	9.98 ± 4.81[g]	7.67 ± 4.89	8.76 ± 2.40[g]	9.21 ± 2.06[g]	6.86 ± 1.78[a,b,c,e,f]	6.24	<0.001
SNR									
Liver	4.92 ± 0.96[b,c,d,e,f,g]	7.29 ± 1.12[a,c,d,g]	6.47 ± 0.92[a,b,d,e,g]	8.3 ± 1.19[a,b,c,f,g]	7.67 ± 1.59[a,c,g]	6.86 ± 1.28[a,d,g]	9.26 ± 1.68[a,b,c,d,e,f]	82.46	< 0.001
Spleen	4.93 ± 0.87[b,c,d,e,f,g]	6.64 ± 0.81[a,c,d,g]	5.83 ± 0.68[a,b,d,e,g]	7.45 ± 0.89[a,b,c,f,g]	7.01 ± 0.93[a,c,d,g]	6.21 ± 0.72[a,d,e,g]	8.35 ± 1.00[a,b,c,d,e,f]	120.73	< 0.001
Kidney	3.69 ± 0.98[b,d,e,f,g]	4.55 ± 1.55[a,e,g]	3.90 ± 1.17[e,f,g]	4.58 ± 1.50[a,e,g]	5.41 ± 1.27[a,b,c,d,f]	4.68 ± 1.07[a,c,e,g]	5.85 ± 1.23[a,b,c,d,f]	25.53	< 0.001
CNR									
Liver	20.94 ± 6.37	19.05 ± 5.86[d,g]	17.75 ± 4.81[d,g]	24.18 ± 7.10[b,c,e,f]	19.40 ± 5.52[a,e,g]	18.07 ± 4.30[d,g]	24.65 ± 6.45[b,c,e,f]	16.31	< 0.001
Spleen	20.20 ± 6.00[c]	18.21 ± 5.54[d,g]	16.97 ± 4.52[a,d,g]	23.13 ± 6.73[b,c,e,f]	18.50 ± 5.27[d,g]	17.22 ± 4.09[d,g]	23.49 ± 6.13[b,c,e,f]	16.61	< 0.001
Kidney	18.11 ± 5.28[g]	16.51 ± 5.21[d,g]	15.40 ± 4.19[d,g]	20.99 ± 6.19[b,c,e,f]	16.87 ± 4.75[d,g]	15.79 ± 3.75[d,g]	21.47 ± 5.57[a,b,c,e,f]	16.48	< 0.001
Calculus									
CT (HU)	1098.50 ± 334.51	1054.1 ± 383.78	1071.93 ± 376.02	1072.16 ± 376.17	1024.38 ± 440.67	1039.07 ± 435.01	1039.36 ± 435.15	0.28	0.94
SD (HU)	157.97 ± 119.8	181.37 ± 109.26	181.58 ± 109.43	179.97 ± 108.84	162.38 ± 124.47	158.67 ± 121.10	158.17 ± 121.66	0.70	0.65
SNR	13.04 ± 16.32	11.46 ± 14.91	10.98 ± 13.35	11.17 ± 13.64	13.66 ± 21.74	13.34 ± 19.48	14.18 ± 22.51	0.38	0.89
CNR	155.11 ± 61.63[d]	139.7 ± 66.32[d]	132.23 ± 58.96[d,g]	179.43 ± 82.54[c,f]	139.74 ± 70.9[d]	131.55 ± 61.14[d,g]	178.75 ± 85.25[c,f]	6.11	< 0.001
Size(cm^3)	3.33 ± 9.97	3.02 ± 9.29	3.02 ± 9.23	3.02 ± 9.22	3.22 ± 9.79	3.18 ± 9.67	3.18 ± 9.65	0.01	1.00

SD: standard deviation, SNR: signal-to-noise ratio, CNR: contrast-to-noise ratio.
a: statistical significance with TNC-AR70, $p < 0.05$.
b: statistical significance with CP-VNC-AR70, $p < 0.05$.
c: statistical significance with CP-VNC-DM, $p < 0.05$.
d: statistical significance with CP-VNC-DH, $p < 0.05$.
e: statistical significance with EP-VNC-AR70, $p < 0.05$.
f: statistical significance with EP-VNC-DM, $p < 0.05$.
g: statistical significance with EP-VNC-DH, $p < 0.05$.

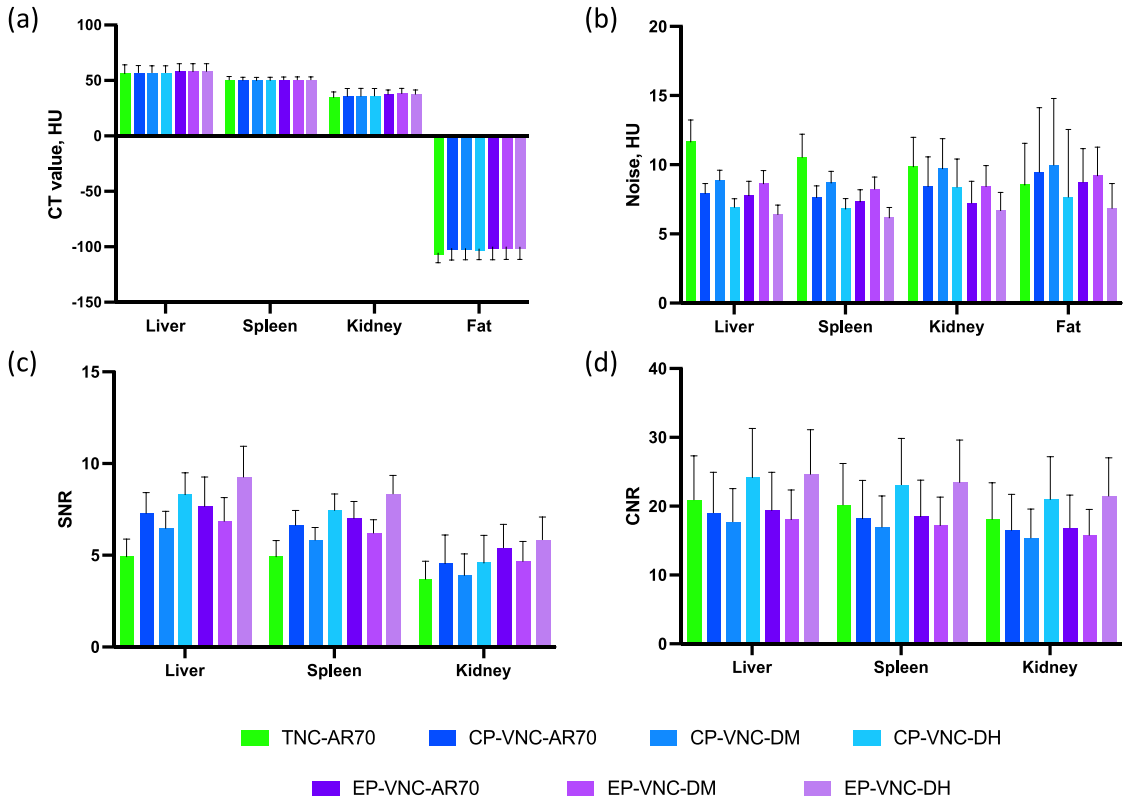

Fig. 1. Comparative analysis of Image quality (a) CT value (b) image noise (c) SNR and (d) CNR.

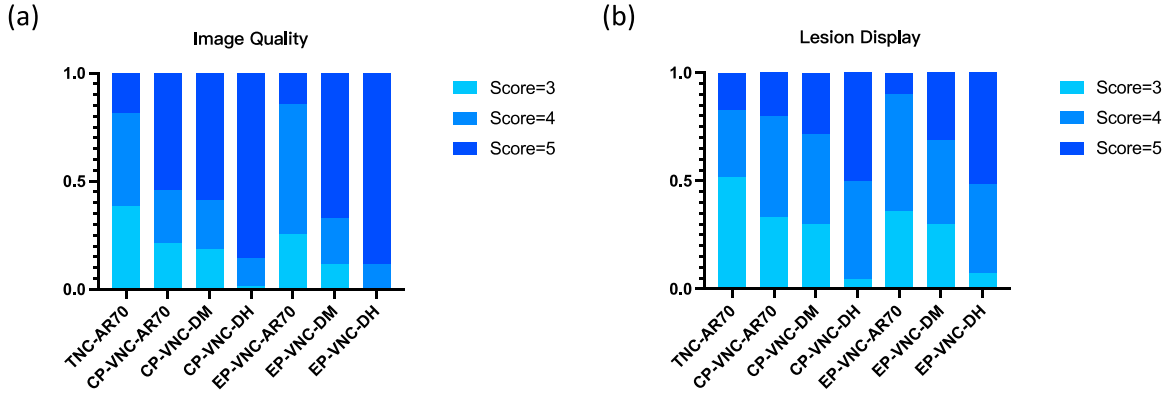

Fig. 2. Comparative analysis of subjective scores between virtual and real noncontrast scans (a) image quality (b) lesion display (scoring using a Likert 5-point method, in which 5 points are the best and more than 3 points represent clinical acceptability).

3.1. Objective image evaluation results

In the objective image quality evaluation, there was no statistical difference in CT values for the liver and spleen among the 7 groups (all $P > 0.05$). For the kidneys and fat CT areas where statistical differences were observed, the differences in CT values between virtual and true non-contrast scans were within 6 Hounsfield Units (HU). Overall, the DLIR group had better image quality than the AR70 group, and the image quality of VNC AR70 images at the same dose was superior to TNC-AR70 images. Specifically, the EP-VNC-DH images had the lowest noise, highest SNR, and CNR (Table 2) ($P < 0.05$). The DH images in the corticomedullary and excretory phases showed lower SD and SNR than DM and TNC-AR70 images. In the comparison of CNR, both CP-VNC and EP-VNC DH images were the highest (Fig. 1).

3.2. Subjective image evaluation results

In the subjective image quality evaluation, EP-VNC-DH performed the best in image quality, while CP-VNC-DH excelled in lesion visibility. It is noteworthy that despite the same reconstruction method, there was a significant difference in image quality between CP-VNC-AR70 and EP-VNC-AR70, which was not observed in CP-VNC-DH and EP-VNC-DH (Fig. 2). The subjective consistency of image quality evaluation by the two physicians was good, with kappa values > 0.8 for both aspects. All 7 images scored ≥ 3 in both image quality and lesion visibility, meeting clinical diagnostic requirements.

3.3. Kidney stone measurement

A total of 70 patients with kidney stones were included, with 9 cases having stones > 5 mm^3, 12 cases with stones measuring 2–5 mm^3, and

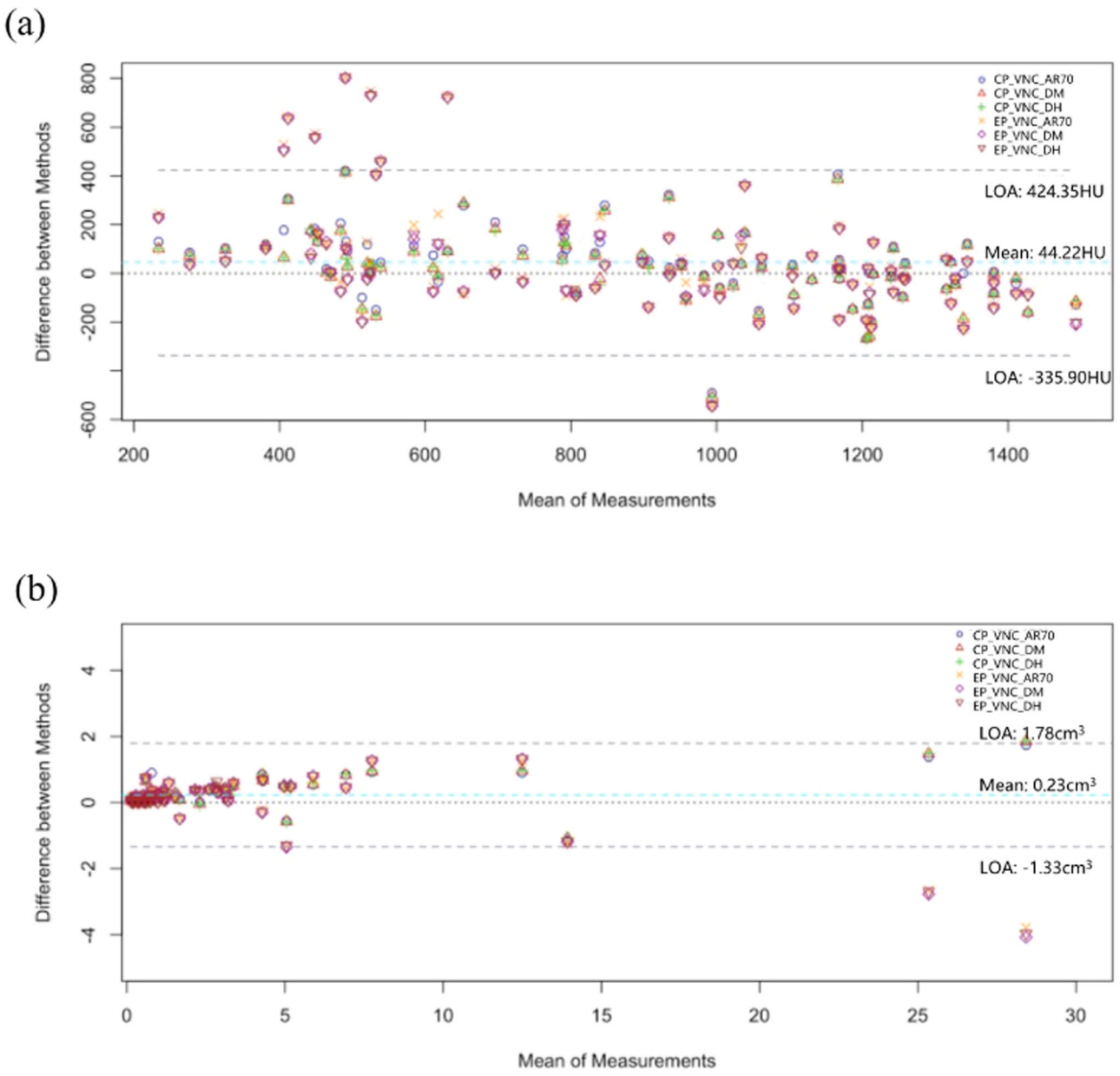

Fig. 3. Bland-Altman comparative analysis of stone measurements between virtual non-contrast scans and true non-contrast scans: (a) CT values, (b) stone volume. limits of agreement (LOA): 95 % confidence interval.

49 cases with stones < 2 mm^3. The stones in all 70 cases were measurable on plain, corticomedullary, and excretory phase scans. There was no statistical difference in stone measurements between the 6 groups of VNC images and the TNC images (all $P > 0.05$). In stone CT values, CP-VNC-DM and CP-VNC-DH measurements were closest to the TNC group, and in stone size, EP-VNC-DM was closest to the TNC group (Fig. 3).

3.4. Comparison of radiation dose

The CTDIvol for routine non-contrast scans ranged from 6.28 to 17.22 mGy, with an average CTDIvol of 9.05 ± 2.63 mGy. The doses for corticomedullary and excretory phase spectral scans were similar, with scan CTDIvol ranging from 6.56 to 17.02 mGy and an average CTDIvol of 8.99 ± 2.75 mGy. There was no statistical difference between the radiation doses of routine non-contrast scans and spectral scans.

4. Discussion

Our study demonstrated that advanced deep learning image reconstruction algorithms shows the ability to elevate the image quality compare to the iterative reconstruction. The use of ASIR-V 70 % as a control group is because 70 % strength provide high level of noise reduction ability without display of severe blocky artifact. The high-level DLIR images exhibited markedly improved noise characteristics, SNR, and CNR when compared to ASIR-V 70 % images. Although medium-level DLIR images showed increased noise and reduced SNR relative to ASIR-V 70 %, the difference in CNR between medium-level DLIR and ASIR-V 70 % images was not statistically significant. Furthermore, the subjective assessments conducted by readers indicated a preference for both high-level and medium-level DLIR images over ASIR-V 70 % images which indicate medium level DLIR can also provide effective noise suppression and image vision at the same time. As shown in Figs. 4 and 5, VNC images from deep learning image reconstruction algorithms had clearer visualization of anatomical structures and small

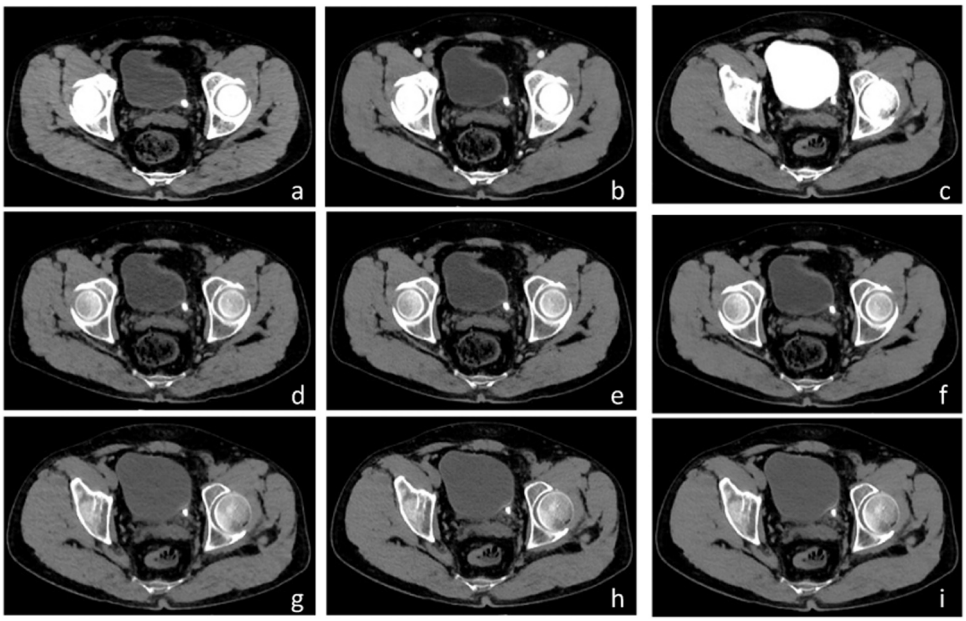

Fig. 4. A 66-year-old man with a urinary disorder to be discharged revealed a stone in the left lower ureter with left hydroureteronephrosis. Figs. a–c were (a) the true contrast enhanced abdominal-pelvic non-contrast images, (b) the 74 keV contrast enhanced images of the corticomedullary phase and (c) the 74 keV contrast enhanced images of the excretory phase. Figs. d–f were (d) the 70 % weighted images of ASIR-V, (e) the midium-level DLIR, and (f) the high-level DLIR of virtual non-contrast corticomedullary phase images. Figs. g–i were (g) the 70 % weighted images of ASIR-V, (h) the medium-level DLIR, and (i) the high-level DLIR of virtual non-contrast excretory phase images.

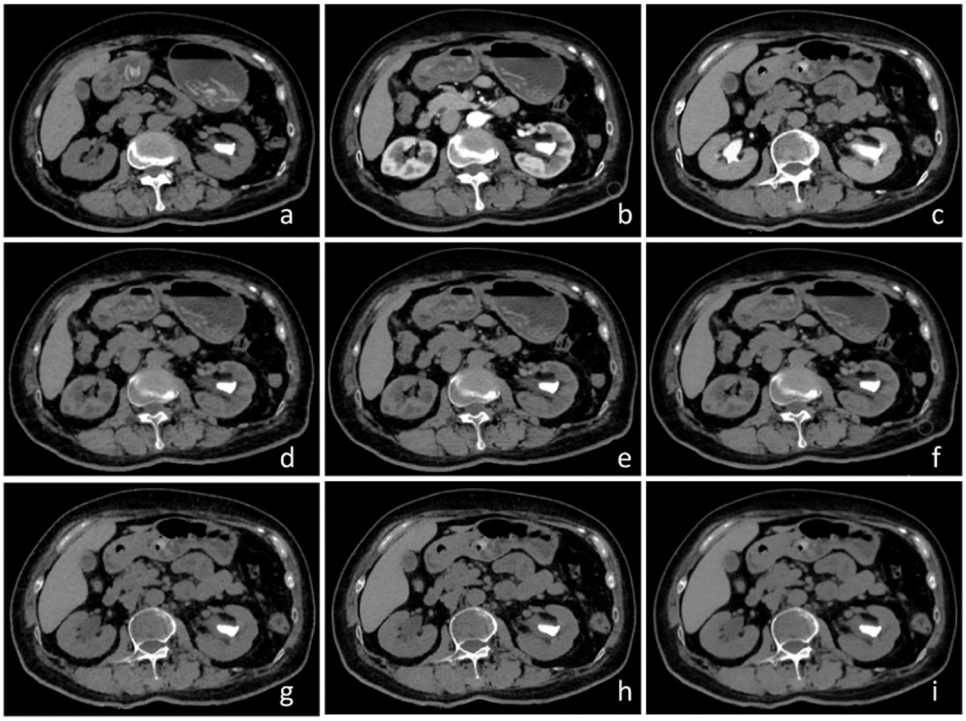

Fig. 5. Female, 69 years old, abdominal pain; Examination reveals multiple stones in the left kidney with mild hydrops. Figs. a–c were (a) the true contrast enhanced abdominal-pelvic non-contrast images, (b) the 74 keV contrast enhanced images of the corticomedullary phase and (c) the 74 keV contrast enhanced images of the excretory phase. Figs. d–f were (d) the 70 % weighted images of ASIR-V, (e) the midium-level DLIR, and (f) the high-level DLIR of virtual non-contrast corticomedullary phase images. Figs. g–i were (g) the 70 % weighted images of ASIR-V, (h) the medium-level DLIR, and (i) the high-level DLIR of of virtual non-contrast excretory phase images.

lesions, and higher contrast. While ASIR-V 70 % images also displayed clear anatomical structures and small lesions, they exhibited more noise and some artifacts. This was consistent with the findings in both phantom and patients studies which demonstrated that unlike the high level iterative algorithms that would produce wax-like artifacts, high level deep learning image reconstruction algorithms produce detailed images without overly smoothing them in non-spectral images and virtual monochromatic images [9,12,13]. These findings underscore the

potential of advanced DLIR algorithms to produce higher-quality images that can improve diagnostic accuracy and reader satisfaction in clinical practice.

The study also showed that CT values of the VNC images generated during both the corticomedullary and excretory phases, as well as three different reconstructions, are consistent with the TNC among the liver, spleen, kidney, and fat except for the excretory phase kidney and fat. Lazar et al. also found that high luminal attenuation during the excretory phase can make the VNC calculation unreliable [15]. This finding suggests that using corticomedullary phase for obtaining VNC images give more accurate CT numbers compared to excretory phase. The findings also shows an improvement result than the previous studies [16–18]. One possible reason for this discrepancy is the improvement in techniques (e.g., kV-mA dual switch spectral techniques on the CT device used in this study) providing more precise and better-matched high and low image pairs in terms of radiation dose and image quality, leading to more accurate material decomposition. Previous studies have shown that VNC images generated between different phases have similar image quality, and our study also confirms this trend, as the three different reconstructions showed similar image quality between the two phases [16].

The VNC images in CTU scans can maintain the visibility of stones and other renal details compare to the TNC images. Stone measurement results also showed that the kidney stone CT values and size values of virtual non-contrast scan images produced by DLIR algorithms were no different from those of the TNC-AR70 images.

Additionally, we further analyzed the virtual non-contrast scan images of the corticomedullary and excretory phases. Although the corticomedullary phase VNC images did not show the ureteral course, they clearly depicted the renal pelvis and calyces; the excretory phase VNC images distinctly displayed the ureteral course without affecting the presence of urinary stones.

Traditional CTU protocols involve multiple scans and high radiation doses, which pose risks to patients, especially considering the radiation-sensitive organs in the lower abdomen. By using DLIR-reconstructed VNC images, it may be possible to reduce the number of required scans and overall radiation exposure while maintaining diagnostic quality. This is particularly beneficial in managing and diagnosing urinary system diseases, where frequent imaging is often necessary.

This study has the following limitations: 1. The sample size was relatively small. 2. The lesion measurement analysis of urinary system diseases only included urinary tract stones. Future studies could further evaluate the value of deep learning image reconstruction algorithms in diagnosing renal tumors and cysts for a comprehensive exploration of urinary system disease diagnosis. 3. Evaluation was only conducted on a single device from a single manufacturer using deep learning spectral image reconstruction algorithms; future research is expected to encompass a more comprehensive study involving multiple manufacturers, scanner types, and imaging centers applying deep learning image reconstruction algorithms to CTU.

In conclusion, the preliminary results of this study suggest that in urinary system CTU examinations, the image quality of virtual non-contrast scan images reconstructed using deep learning image reconstruction algorithms is superior to true non-contrast scans using the conventional ASIR-V70 %. Combining the use of corticomedullary DLIR reconstructed virtual non-contrast scan images has the potential for dose reduction while providing accurate clinical diagnosis for urinary stones.

CRediT authorship contribution statement

Hong Zhu: Writing – review & editing, Writing – original draft, Methodology, Investigation, Formal analysis, Data curation. **Jing Fan:** Writing – review & editing, Writing – original draft, Supervision, Methodology, Investigation, Formal analysis, Data curation, Conceptualization. **Xiaomeng Shi:** Writing – review & editing, Formal analysis. **Deyan Kong:** Writing – review & editing, Data curation. **Jiale Qian:** Data curation.

Ethical statement

This study was approved by the ethics committee of our hospital. All participants gave written informed consent before final inclusion.

Funding statement

The authors state that this work has not received any funding.

Declaration of Competing Interest

The authors declare the following financial interests/personal relationships which may be considered as potential competing interest: Jing Fan reports was provided by Ruijin Hospital Shanghai Jiaotong University School Of Medicine. If there are other authors, they declare that they have no known competing financial interests or personal relationships that could have appeared to influence the work reported in this paper.

References

[1] X. Zhang, J. Chen, N. Yu, Z. Ren, Q. Tian, X. Tian, Y. Jia, T. He, C. Guo, Reducing contrast medium dose with low photon energy images in renal dual-energy spectral CT angiography and adaptive statistical iterative reconstruction (ASIR), BJR 94 (2021) 20200974, https://doi.org/10.1259/bjr.20200974.

[2] S. Zeng, M. Du, Y. Yu, S. Huang, D. Zhang, X. Cui, C.F. Dietrich, Ultrasound, CT, and MR imaging for evaluation of cystic renal masses, J. Ultrasound Med. 41 (2022) 807–819, https://doi.org/10.1002/jum.15762.

[3] L.L. Geyer, U.J. Schoepf, F.G. Meinel, J.W. Nance, G. Bastarrika, J.A. Leipsic, N. S. Paul, M. Rengo, A. Laghi, C.N. De Cecco, State of the art: iterative CT reconstruction techniques, Radiology 276 (2015) 339–357, https://doi.org/10.1148/radiol.2015132766.

[4] C.E. Althoff, R.W. Günther, B. Hamm, M. Rief, Intra-arterial ultra low iodine CT angiography of renal transplant arteries, Cardiovasc. Interv. Radiol. 37 (2014) 1062–1067, https://doi.org/10.1007/s00270-014-0838-9.

[5] M.K. Virarkar, S.S.R. Vulasala, A.V. Gupta, D. Gopireddy, S. Kumar, M. Hernandez, C. Lall, P. Bhosale, Virtual non-contrast imaging in the abdomen and the pelvis: an overview, Semin. Ultrasound CT MRI 43 (2022) 293–310, https://doi.org/10.1053/j.sult.2022.03.004.

[6] Y. Cheng, J. Sun, J. Li, Y. Han, X. Zhang, L. Zhang, J. Zheng, H. He, J. Yang, J. Guo, The added value of virtual unenhanced images obtained from dual-energy CT urography in the detection and measurement of urinary stone, Urology 166 (2022) 118–125, https://doi.org/10.1016/j.urology.2022.02.029.

[7] G. Ma, D. Han, S. Dang, N. Yu, Q. Yang, C. Yang, C. Jin, Y. Dou, Replacing true unenhanced imaging in renal carcinoma with virtual unenhanced images in dual-energy spectral CT: a feasibility study, Clin. Radiol. 76 (2021) 81.e21–81.e27, https://doi.org/10.1016/j.crad.2020.08.026.

[8] M. Meyer, R.C. Nelson, F. Vernuccio, F. González, A.E. Farjat, B.N. Patel, E. Samei, T. Henzler, S.O. Schoenberg, D. Marin, Virtual unenhanced images at dual-energy CT: influence on renal lesion characterization, Radiology 291 (2019) 381–390, https://doi.org/10.1148/radiol.2019181100.

[9] J. Greffier, A. Viry, Y. Barbotteau, J. Frandon, M. Loisy, F. De Oliveira, J.P. Beregi, D. Dabli, Phantom task-based image quality assessment of three generations of rapid kV-switching dual-energy CT systems on virtual monoenergetic images, Med. Phys. 49 (2022) 2233–2244, https://doi.org/10.1002/mp.15558.

[10] J. Zhong, H. Shen, Y. Chen, Y. Xia, X. Shi, W. Lu, J. Li, Y. Xing, Y. Hu, X. Ge, D. Ding, Z. Jiang, W. Yao, Evaluation of image quality and detectability of deep learning image reconstruction (DLIR) algorithm in single- and dual-energy CT, J. Digit Imaging 36 (2023) 1390–1407, https://doi.org/10.1007/s10278-023-00806-z.

[11] T. Lee, J.M. Lee, J.H. Yoon, I. Joo, J.S. Bae, J. Yoo, J.H. Kim, C. Ahn, J.H. Kim, Deep learning–based image reconstruction of 40-keV virtual monoenergetic images of dual-energy CT for the assessment of hypoenhancing hepatic metastasis, Eur. Radiol. 32 (2022) 6407–6417, https://doi.org/10.1007/s00330-022-08728-0.

[12] A. Delabie, R. Bouzerar, R. Pichois, X. Desdoit, J. Vial, C. Renard, Diagnostic performance and image quality of deep learning image reconstruction (DLIR) on unenhanced low-dose abdominal CT for urolithiasis, Acta Radiol. 63 (2022) 1283–1292, https://doi.org/10.1177/02841851211035896.

[13] Y.J. Yoo, I.Y. Choi, S.K. Yeom, S.H. Cha, Y. Jung, H.J. Han, E. Shim, Evaluation of abdominal CT obtained using a deep learning-based image reconstruction engine compared with CT using adaptive statistical iterative reconstruction, J. Belg. Soc. Radiol. 106 (2022) 15, https://doi.org/10.5334/jbsr.2638.

[14] J. Park, J. Shin, I.K. Min, H. Bae, Y.-E. Kim, Y.E. Chung, Image quality and lesion detectability of lower-dose abdominopelvic CT obtained using deep learning image reconstruction, Korean J. Radiol. 23 (2022) 402, https://doi.org/10.3348/kjr.2021.0683.

[15] M. Lazar, H. Ringl, P. Baltzer, D. Toth, C. Seitz, B. Krauss, E. Unger, S. Polanec, D. Tamandl, C.J. Herold, M. Toepker, Protocol analysis of dual-energy CT for optimization of kidney stone detection in virtual non-contrast reconstructions, Eur. Radiol. 30 (2020) 4295–4305, https://doi.org/10.1007/s00330-020-06806-9.

[16] L. Lehti, M. Söderberg, P. Höglund, J. Wassélius, Comparing arterial- and venous-phase acquisition for optimization of virtual noncontrast images from dual-energy computed tomography angiography, J. Comput. Assist. Tomogr. 43 (2019) 770–774, https://doi.org/10.1097/RCT.0000000000000903.

[17] W. Kazimierczak, N. Kazimierczak, Z. Serafin, Quality of virtual-non-contrast phases derived from arterial and delayed phases of fast-kVp switching dual-energy CT in patients after endovascular aortic repair, Int. J. Cardiovasc. Imaging 39 (2023) 1805–1813, https://doi.org/10.1007/s10554-023-02887-x.

[18] S. Verstraeten, J. Ansems, W.V. Ommen, D.V.D. Linden, F. Looijmans, E. Tesselaar, Comparison of true non-contrast and virtual non-contrast images in the characterization of renal lesions using detector-based spectral CT, Br. J. Radiol. 96 (2023) 20220157, https://doi.org/10.1259/bjr.20220157.